Syracuse University
SURFACE

Physics | College of Arts and Sciences

3-30-2011

# The Shrinking Instability of Toroidal Liquid Droplets in the Stokes Flow Regime

Mark Bowick
*Department of Physics, Syracuse University, Syracuse, NY*, bowick@physics.syr.edu

Zhenwei Yao
*Syracuse University*

Follow this and additional works at: http://surface.syr.edu/phy

Part of the Physics Commons

Repository Citation
Bowick, Mark and Yao, Zhenwei, "The Shrinking Instability of Toroidal Liquid Droplets in the Stokes Flow Regime" (2011). *Physics.* Paper 136.
http://surface.syr.edu/phy/136

This Article is brought to you for free and open access by the College of Arts and Sciences at SURFACE. It has been accepted for inclusion in Physics by an authorized administrator of SURFACE. For more information, please contact surface@syr.edu.

# The shrinking instability of toroidal liquid droplets in the Stokes flow regime

Zhenwei Yao and Mark J. Bowick
*Department of Physics, Syracuse University, Syracuse, New York 13244-1130, USA*

We analyze the stability and dynamics of toroidal liquid droplets. In addition to the Rayleigh instabilities akin to those of a cylindrical droplet there is a shrinking instability that is unique to the topology of the torus and dominates in the limit that the aspect ratio is near one (fat tori). We first find an analytic expression for the pressure distribution inside the droplet. We then determine the velocity field in the bulk fluid, in the Stokes flow regime, by solving the biharmonic equation for the stream function. The flow pattern in the external fluid is analyzed qualitatively by exploiting symmetries. This elucidates the detailed nature of the shrinking mode and the swelling of the cross-section following from incompressibility. Finally the shrinking rate of fat toroidal droplets is derived by energy conservation.

PACS numbers: 47.20.Dr

arXiv:1011.3437v3 [cond-mat.soft] 30 Mar 2011

Liquid droplets of various shapes are ubiquitous in nature pure and applied. They are found in rain, clouds, paint, lubricants, inks, dyes and oil [1, 2] and are being increasingly exploited in microfluidics [3]. The instabilities of liquid droplets have attracted attention since the beginning of the 19th century [4–9]. Early work of Plateau showed that a long cylindrical liquid droplet is unstable to capillary wave deformations of wavelength exceeding the droplet circumference. Rayleigh subsequently determined the most unstable capillary mode by solving the Navier-Stokes equation [10, 11]. Purely planar liquid droplets are, in contrast, stable since capillary waves always increase the droplet surface area and hence the free energy [12]. Droplet instabilities thus probe the combined influence of the three-dimensional geometry of the droplets and their surface tension [4].

In this paper we study the instability of liquid droplets in the form of three-dimensional axially symmetric solid tori, inspired by recent experiments in which bulk liquid tori are created by extruding water or glycerin through a metallic needle into a rotating bath of viscous silicone oil [13]. Thin toroidal droplets exhibit Rayleigh instabilities analogous to those of the cylinder [10, 14, 15], with the additional requirement that the most unstable mode has wavelength $\lambda_c$ commensurate with the outer circumference of the torus. When the outer circumference is an integer (n) times $\lambda_c$, the toroidal droplet eventually fissions into n solid spherical droplets (three-dimensional balls). Thus the change in topology of the droplet (solid torus breaks up into n balls) is governed by a Bohr quantization condition with the final number of balls playing the role of the principal quantum number n. Toroidal droplets also exhibit a fundamentally different type of instability in which the torus shrinks to close its interior hole, eventually becoming a single ball. This instability is a signature of the topological character of the torus and does not exist for a cylinder. Although it is present for a torus of any aspect ratio, it is preempted by the Rayleigh instability unless the torus is sufficiently fat (see Appendix B).

The outline of this paper is as follows: we first analyze the shrinking instability of toroidal droplets by minimizing a free energy controlled by interfacial surface tension. We then derive the pressure distribution driving bulk flow of the fluid. The shrinking mode is then examined in more depth via the Stokes equation, which is the large Ohnesorge number ($Oh \equiv \eta/\sqrt{\rho L \sigma} >> 1$) limit of the Navier-Stokes equation. The biharmonic equation for the stream function determines the velocity field inside the toroidal liquid droplet. The shrinking of the droplet and simultaneous swelling of the cross-section from volume conservation are clearly revealed in the flow. Finally, we calculate the shrinking speed by balancing the rate of free energy gain with the viscous dissipation rate.

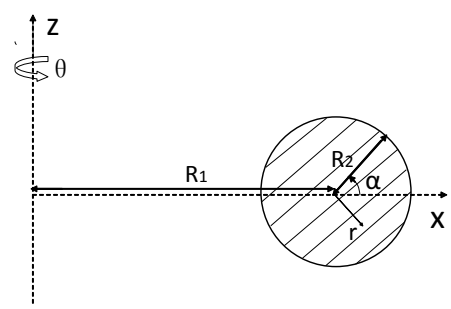


FIG. 1: Schematic of coordinates for a solid torus generated by rotating a circular disk of radius $R_2$, centered a distance $R_1$ from the origin, around the vertical (z) axis.

A three-dimensional axially symmetric solid torus is characterized by coordinates $\{u^1 = \alpha, u^2 = \theta, u^3 = r\}$, as shown in Fig.1. Here $\alpha$ is the angle around the tube, $\theta$ is the azimuthal angle around the z-axis, and $r$ is the radial coordinate of the tube. The central circle of the solid torus with radius $R_1$ (at $r = 0$) will be called the reference circle of the solid torus. The outer radius of the tube is denoted $R_2$. The aspect ratio of the toroidal surface is then $\phi = R_1/R_2$. The non-zero components of the metric tensor of the solid torus are $g_{11} = r^2$, $g_{22} = (R_1 + r\cos\alpha)^2$ and $g_{33} = 1$.

The instability of a toroidal liquid droplet to shrinking can be seen in terms of the free energy $F = \sigma A$. In

the shrinking process, $R_1$ decreases and $R_2$ increases due to volume conservation. The change of free energy with radius is

$$\frac{dF}{dR_1} = 2\pi^2 \sigma R_2 > 0. \tag{1}$$

Thus toroidal liquid droplets shrink to reduce the free energy. Although this static analysis reveals the shrinking mode, the free energy alone does not provide a complete description of the system. In particular, determining the shrinking rate requires a study of droplet hydrodynamics.

We first analyze the pressure distribution in a toroidal droplet to understand the driving force for bulk flow. Taking the divergence of the Navier-Stokes equation for an incompressible fluid shows that the pressure must be harmonic

$$\Delta p(r, \alpha) = 0 \ . \tag{2}$$

The boundary condition is given by the distribution of Laplace pressure on the interface between the inner and outer fluids

$$p - p_0 = \sigma H, \tag{3}$$

where H is the mean curvature $H = \frac{R_1 + 2R_2 \cos\alpha}{R_2(R_1 + R_2 \cos\alpha)}$. For simplicity, we first consider the external pressure $p_0$ as constant. The problem of solving for the pressure distribution in the bulk fluid is then reduced to solving Laplace's equation, Eq.(2), with the specified boundary condition. The Laplace pressure drop from the exterior ($\alpha = 0$) to the interior ($\alpha = \pi$) of the torus is given by $P(\alpha = 0) - P(\alpha = \pi) = 2\sigma \frac{1}{R_2} \frac{\phi}{\phi^2 - 1}$ and is a measure of the asymmetry of the torus. Since $\phi > 1$, the Laplace pressure on the exterior of the toroid is always bigger than on the interior. One also sees that the asymmetry is more pronounced for a fat torus with aspect ratio $\phi$ approaching one. In the limit $\phi \to \infty$, a toroid approaches a solid cylinder and the asymmetry as well as the shrinking mode disappear. Note that for the opposite case of constant pressure in the inner fluid, the pressure in the outer fluid will fall from the interior to the exterior of the torus. The outer fluid will therefore flow outward and the inner fluid will correspondingly flow inward, shrinking the droplet. Shrinking is thus a universal feature of one toroidal fluid inside another.

Laplace's equation for the pressure Eq.(2) separates in the coordinates $\{\rho, \varphi, \theta\}$[16, 17] defined by

$$\vec{x}(\rho, \varphi, \theta) = \begin{pmatrix} \frac{a \sinh\rho \cos\theta}{\cosh\rho - \cos\varphi} \\ \frac{a \sinh\rho \sin\theta}{\cosh\rho - \cos\varphi} \\ \frac{a \sin\varphi}{\cosh\rho - \cos\varphi} \end{pmatrix},$$

where $a = r \sinh\rho$.

Exploiting azimuthal symmetry and imposing the requirement that the pressure be finite as one approaches the reference circle, the physically acceptable solution takes the form [17]

$$p = \sqrt{\cosh\rho - \cos\varphi} \sum_{p \in \mathbb{Z}} \alpha_p \mathrm{Re}[Q_{p-1/2}(\cosh\rho)] \cos(p\varphi) \tag{4}$$

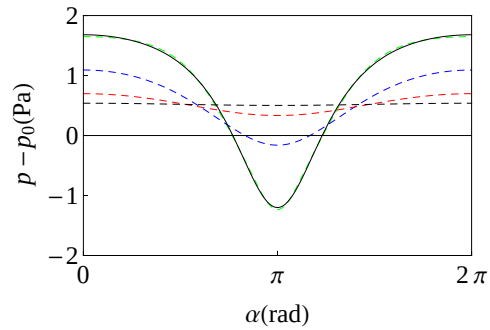


FIG. 2: The pressure $p(r, \alpha)$ vs. angle $\alpha$ at different radial distances away from the reference circle for $R_1 = 5$ mm and aspect ratio $\phi = R_1/R_2 = 1.5$. The solid black curve is the pressure distribution on the boundary $p = \sigma H$. Green curve: $r = R_1/1.5$ (boundary). Blue curve: $r = R_1/3$. Red curve: $r = R_1/10$. Dashed Black curve: $r = R_1/100$. The green curve fits the exact pressure on the boundary very well.

where $Re[Q_{p-1/2}(x)]$ is the real part of the associated Legendre function of the second kind. The coefficients $\alpha_p$ can be determined by imposing the boundary condition in Eq.(3). The pressure distribution inside the droplet is plotted in Fig.2 for aspect ratio $\phi = 1.5$, surface tension $\sigma = 4 \times 10^{-3}$ N/m and $R_1 = 5$ mm. The pressure clearly drops from the exterior ($\alpha = 0, 2\pi$) to the interior ($\alpha = \pi$). This pressure gradient drives the fluid towards the center of the toroid. As $r$ decreases the pressure distribution becomes more isotropic ($\alpha$-independent). Note that only the $p = 0$ mode in Eq.(4) contributes to the pressure near the reference circle. This enables us to study the behavior of the fluid near the reference circle analytically. By inserting the zero mode in Eq.(4) into the Stokes equation one can determine the velocity field near the reference circle in $\{x, z\}$ coordinates: $v_x = v_\alpha \sin\alpha - v_r \cos\alpha = c$, and $v_z = v_\alpha \cos\alpha + v_r \sin\alpha = 0$. The velocity field near the reference circle is uniform towards the center of the toroid.

We now turn to the velocity distribution in a viscous toroidal liquid droplet. In this regime of large Ohnesorge number the Navier-Stokes equation reduces to the Stokes equation

$$\Delta \vec{v} = \frac{1}{\eta} \nabla p, \tag{5}$$

where $\eta$ is the fluid viscosity. Here viscous dissipation dominates over kinetic energy damping:

$$\frac{\dot{E}_{kin}}{\dot{E}_{visc}} = \frac{d[\frac{1}{2} \int \rho v^2 dV]/dt}{\int dV \sigma'_{ij} \nabla^i v^j} \propto \frac{\rho L \sigma}{\eta^2} << 1, \tag{6}$$

where $\sigma'_{ij} = \eta(\nabla_i v_j + \nabla_j v_i)$ is the viscous stress tensor. Since the characteristic speed of the fluid is much smaller than the speed of sound, we can treat the fluid as incompressible ($\nabla \cdot \vec{v} = 0$)[18]. For incompressible fluids one can write the velocity field as the curl of a vector

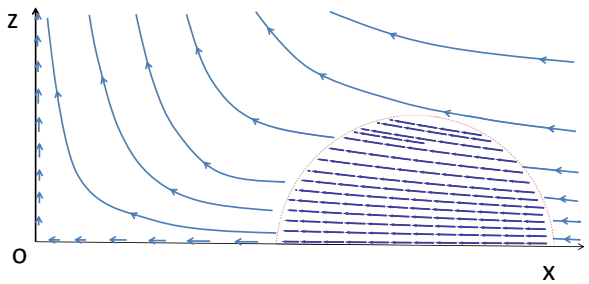


FIG. 3: The velocity field inside and outside a cross-section of a toroidal liquid droplet. The dashed semi-circle is the interface of two distinct fluids. The velocity field inside the droplet is calculated by solving the biharmonic equation. The external flow pattern is schematically plotted by imposing boundary conditions and exploiting symmetry. Parameters are mode number $\nu = 1$, $R_1 = 5$ mm and $R_2 = 2$ mm.

potential $\vec{\psi}$ ($\vec{v} = \nabla \times \vec{\psi}$) leading directly to

$$\Delta^2 \vec{\psi} = 0. \tag{7}$$

The complete velocity field can be obtained by solving the biharmonic vectorial equation Eq.(7) which reduces to a simplified scalar differential equation in the $\{\rho, \varphi, \theta\}$ coordinates[19]

$$E^2(E^2\psi) = 0, \tag{8}$$

where $\psi$, the stream function, is the only non-zero component $\psi_\theta$ of the vector potential $\vec{\psi}$ and the second-order partial differential operator $E$ is given by $E^2 = wh^2[\partial_\rho(\frac{1}{w}\partial_\rho) + \partial_\varphi(\frac{1}{w}\partial_\varphi)]$, with $w = a\ \sinh(\rho)/[\cosh(\rho) - \cos(\varphi)]$ and $h = [\cosh(\rho) - \cos(\varphi)]/a$. Imposing the physical requirements that approaching the reference circle $v_x$ tends to a finite value and $v_z \to 0$ (reflection symmetry) yields the complete solution

$$\psi = \frac{a \sinh\rho}{(\cosh\rho - \cos\varphi)^{3/2}} \sum_{\nu=-\infty}^{+\infty} c_\nu \sin(\nu\varphi) Q^1_{\nu-3/2}(\cosh\rho) \tag{9}$$

Note that $v_x \to -\frac{\pi c_1}{2\sqrt{2}}$ and $v_z \to 0$ as $\rho \to \infty$ ($r \to 0$). Thus only the $\nu = 1$ mode contributes to the flow near the reference circle. The coefficients $c_\nu$ in Eq.(9) can be determined by matching to the velocity field on the interface. Assuming that high viscosity fixes the fluid particles on the interface to move with the interface as it shrinks, the boundary conditions are found to be $v_{x0} = V(1 - \frac{x_0}{2\ R_1})$ and $v_{z0} = -\frac{V\ z_0}{2\ R_1}$, where $x_0$ and $z_0$ denote spatial points on the boundary and $V \equiv dR_1/dt$. The point $(x = 0, z = 0)$ is the center of the cross section. The $\nu = 1$ mode is sufficient to fit this boundary condition.

The velocity field inside the droplet in the laboratory frame is plotted in Fig.3. The shrinking of the droplet is clearly indicated by the inward directed flow inside the droplet. One also sees that outer fluid within the toroidal hole is squeezed out. Further insight is provided by plotting the velocity field (see Fig.4) inside the droplet in a reference frame comoving with the shrinking of the droplet. The swelling of the cross section resulting from volume conservation is clearly visible.

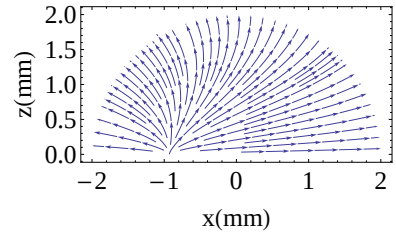


FIG. 4: The velocity field inside the toroidal droplet of Fig.3 in a comoving reference frame shrinking with the droplet. The swelling of the cross section is readily inferred.

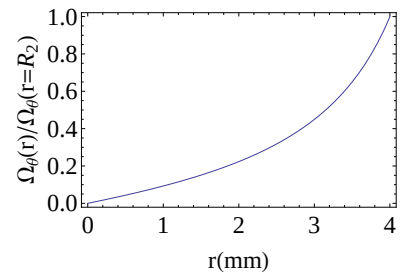


(a)

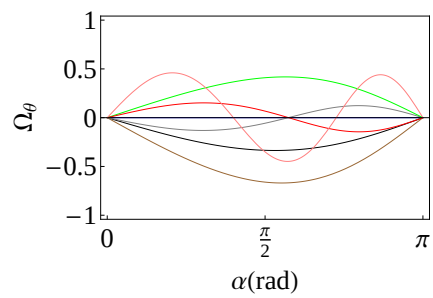


(b)

FIG. 5: (a) The vorticity $\Omega_\theta(r)/\Omega_\theta(r = R_2)$ versus $r$. Parameters: $\nu = 1$, $c_1 = 1$, $\alpha = 1$ rad, $R_1 = 5$ mm and $R_2 = 4$mm . The vorticity field falls to zero at the reference circle. (b) $\Omega_\theta$ versus angle $\alpha$ for modes $\nu$ in the range $(-3, 3)$. The vorticity $\Omega_\theta$ is rescaled to show different modes in the same figure. Parameters: $\phi = 5, a = 1$. Blue curve: $\nu = 0$ (vorticity vanishes). Black curve: $\nu = 1$. Brown curve: $\nu = 2$. Gray curve: $\nu = 3$. Green curve: $\nu = -1$. Red curve: $\nu = -2$. Pink curve: $\nu = -3$. Note that the number of peaks or valleys is determined by the mode number $\nu$.

The vorticity field, $\vec{\Omega} \equiv \nabla \times \vec{v} = -\Delta\vec{\psi}$ is plotted in Fig.5 which shows its only non-zero component $\Omega_\theta$ as a function of $r$ and $\alpha$ respectively. Fig.5(a) shows that the vorticity field is only significant near the boundary – it decays rapidly as one approaches the reference circle. Fig.5(b) shows $\Omega_\theta$ versus $\alpha$ for $\nu \in [-3, 3]$. The vorticity field vanishes at $\alpha = 0$ and $\pi$ due to its odd parity. The sign of $\Omega_\theta$ reflects the chiral property of vortices. The number of peaks and valleys on the $z > 0$ plane (i.e.,

$\alpha \in [0, \pi]$) is

$$n = \begin{cases} -\nu, & \nu < 0 \\ \nu - 1, & \nu > 1 \\ 1, & \nu = 1, \end{cases}$$

and is therefore completely determined by the mode $\nu$.

In the process of shrinking the free energy gained is dissipated in viscous damping. By equating the rate of change of the free energy, Eq.(1), to the viscous dissipation rate we can obtain the shrinking speed. We focus here on the experimentally explored case of a low viscosity ($\eta_i$) inner fluid immersed in a viscous ($\eta_o$) outer bath [13]. In this case the dissipation occurs almost entirely in the outer fluid. Applying Stokes' equation for an incompressible fluid the dissipation rate can be separated into two parts

$$\dot{E}_{vis} = -\int dV \sigma'_{ij} \partial_i v_j = -\int df_i \sigma'_{ij} v_j + \int dV v_j \partial_i \sigma'_{ij} \ . \tag{10}$$

Here $df_i$ is the $i$ component of the area element of the interface. The first term is the heat flux on the fluid boundary and the second term is the dissipation rate inside the bulk fluid. The second term can be related to the vorticity: $\int v_j \partial_i \sigma'_{ij} dV = \eta \int v_j \Delta v_j dV = -\eta \int \vec{v} \cdot (\nabla \times \vec{\Omega}) dV$. Since the Reynolds number of the external fluid is very small in the experimental setup ($Re \approx 10^{-4}$ [13]), we may take the external flow to be as irrotational (vanishing vorticity) by recalling the experiment of flow through a cylindrical solid: an irrotational-rotational flow transition occurs at $Re \sim 1$, below which the flow is irrotational [20]. In the shrinking process, the toroidal droplet moves in the external fluid. This is equivalent to flow through the toroidal droplet. Since the viscosity of the internal fluid is very small in this case, the internal dissipation can be neglected. Thus we need to calculate only the surface integral in Eq.(10) to obtain the dissipation rate. We need the viscous stress on the boundary to evaluate the surface integral. Rotational symmetry and the limiting condition $\eta_i/\eta_o \ll 1$ imply both $\sigma'_{r\theta}$ and $\sigma'_{r\alpha}$ vanish at the interface. To determine $\sigma'_{rr} = 2\eta_o \partial_r v_r$ we need the gradient of $v_r$ at the interface. Assuming that the fluid particles *near* the boundary move together with the interface during shrinking, as a result of the viscous external fluid, we have

$$\partial_r v_r|_{interface} = \frac{6R_1}{R_2^2} \dot{R}_2 \cos\alpha. \tag{11}$$

Inserting Eq.(11) along with the velocity field on the interface into the surface term of Eq.(10) yields

$$\dot{E}_{vis} = -24\pi^2 \eta_o ((\frac{R_1}{R_2})^2 - \frac{1}{2}) R_2 \dot{R}_1 \dot{R}_2 \ . \tag{12}$$

By equating the rate of change of the free energy from Eq.(1) and the dissipation rate Eq.(12), we have

$$\dot{R}_2(t) = \frac{v_s}{12} \frac{1}{\phi^2(t) - 1/2} \tag{13}$$

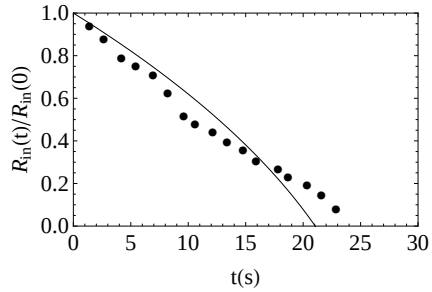


FIG. 6: The time evolution of the normalized inner droplet radius $R_{in}(t)/R_{in}(0)$ for initial aspect ratio 1.4. The theoretical result is the solid curve and the experimental data points are taken from Ref.[13]. Parameters: $R_1(0)$= 3 mm; $v_s = \sigma/\eta_o = 133$ $\mu$m/s.

and the interior hole of the droplet decreases in size according to

$$\dot{R}_{in}(t) = -\frac{v_s}{12} \frac{2\ \phi(t) + 1}{\phi^2(t) - 1/2}, \tag{14}$$

where $\phi(t) = R_1(t)/R_2(t)$ and $v_s = \sigma/\eta_o$. The shrinking speed is controlled by the aspect ratio of the droplet, in accord with experimental observations [13]. In the limit of infinite aspect ratio (the cylinder) the shrinking speed vanishes, as required. The constant 1/2 in the denominator of Eq.(13) plays an important role in the limit that the aspect ratio approaches one (fat tori). The plot of $R_{in}(t)/R_{in}(0)$ versus $t$ is shown in Fig.6 for an initial aspect ratio $R_1(0)/R_2(0) = 1.4$, $\eta_i/\eta_o = 1/30,000$, $\sigma = 4$ mN/m, $R_1(0) \approx$ 3 mm and $\eta_i = 10^{-3}$ kg/(m $\cdot$ s). For these parameters $v_s = \sigma/\eta_o \approx 133$ $\mu$m/s. Fig.6 shows that droplets shrink with roughly constant speed, as found in [13]. Our results predict that it would take about 21 s (aspect ratio 1.4) and 50 s (aspect ratio 1.9) for a toroidal droplet to shrink to close the inner hole of toroid, in qualitative agreement with the experimental values of 25 s and 38 s respectively. Thus thinner toroidal droplets shrink more slowly, consistent with experimental observations [13].

Our energy conservation approach to determining the shrinking speed can also be applied to a 2-dimensional system where it yields an analytical result. Consider a shrinking hole on a liquid film. The limiting case of a shrinking toroidal liquid droplet with $R_{in} \to 0$ and $\eta_i/\eta_o >> 1$ can be modelled as such a 2-dimensional system, since the dynamics of the hole becomes independent of the fluid far away from the hole. As the hole shrinks, a flow will be induced outside the hole on the film. In the Stokes flow regime, the velocity field can be derived analytically in the polar coordinates $\{\rho, \theta\}$ as $v_\rho = \frac{1}{\rho} r(t)\dot{r}(t)$ and $v_\theta = 0$. By energy conservation, the shrinking speed of the hole can also be derived analytically. By equating the rate of change of the line energy $\dot{E}_s = \frac{dE_s}{dt} = 2\pi\gamma\ \dot{r}$ and the viscous dissipation rate $\dot{E}_{vis} = -\int \rho d\rho d\theta (\sigma'^{\rho\rho} \partial_\rho v_\rho) = -2\pi\eta\ \dot{r}^2$, we have $\dot{r} = \frac{\gamma}{\eta}$, where $\eta$ is the viscosity of fluid and $\gamma$ is the line tension.

We expect that the formalism employed here will have a variety of applications to the dynamics of fluid interfaces. It may also be extended to liquid crystalline droplets where the interplay of liquid crystalline order and the shape of the droplet should be very rich.


### Acknowledgements

We thank Xiangjun Xing for extensive discussions and Alberto Fernández-Nieves for introducing us to his beautiful experiments on toroidal droplets. This work was supported by the National Science Foundation grant DMR-0808812 and by funds from Syracuse University.


## Appendix

### A. The shape of cross section

So far we have assumed that droplets remain perfectly circular in cross-section as they shrink. Here we show that this assumption is well justified.

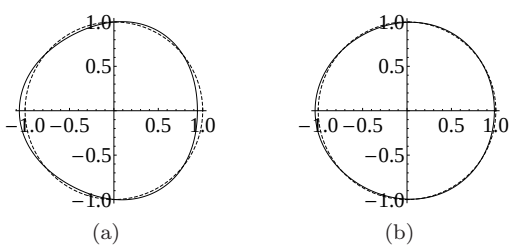


FIG. 7: Minimum energy cross-sectional shapes within a two parameter family of possible shapes (see Eq.(A.1)). The dashed curves are the unperturbed circular shapes: (a) aspect ratio 10 (thin torus) and (b) aspect ratio 2 (fat torus). Parameters: $R_2 = 1$.

The shape of a toroidal liquid droplet is characterized by the radii $R_1$ and $R_2$ which may in general vary with $\alpha$ and $\theta$. Retaining azimuthal symmetry we consider the following ansatz for $R_2$ at a fixed time:

$$R_2(\alpha) = a + c_2 P_2(\cos\alpha) + c_3 P_3(\cos\alpha). \tag{A.1}$$

The second term describes an ellipse which is symmetric about z axis, while the third term describes a shape with three round corners, which is asymmetric about the z-axis (we are ignoring the shrinking mode here, described by a $P_1(\cos\alpha)$ term). The shape of the droplet is specified by points in the $\{c_2, c_3 | c_2, c_3 \in [-b, b]\}$ space.

We numerically search for the ground state in the $\{c_2, c_3 | c_2, c_3 \in [-b, b]\}$ space for which

$$L = A - A_0 + \lambda |V - V_0| \tag{A.2}$$

is minimized, where $V_0$ and $A_0$ are the volume and surface area of the unperturbed droplet. $\lambda$ is set to be large to impose volume conservation. We take $a = 1$ and $b = 0.2$.

For tori with typical aspect ratios $R_1/R_2 = 10$ and 2, we find the ground states in the $\{c_2, c_3 | c_2, c_3 \in [-b, b]\}$ space shown in Fig.7. The cross-sections are very close to circular. In the experimental work of [13] this is also true.

### B. Rayleigh instability vs shrinking mode

It is observed experimentally[13] that the Rayleigh instability disappears for sufficiently fat solid tori ($R_1(t = 0)/R_2(t = 0) \lesssim 2$) whereas the shrinking mode is present for all aspect ratios. Here we derive a lower bound on the aspect ratio for the emergence of the Rayleigh instability.

Two conditions must be satisfied for the Rayleigh instability: (1) modes with wavelength $\lambda > \lambda_c$, where $\lambda_c$ is the minimum wavelength of the Rayleigh instability mode and (2):

$$u_k(t = t_1) \gtrsim R_2(t = 0), \tag{B.1}$$

where $u_k$ is the perturbation amplitude and $t_1$ is the lifetime of the shrinking droplet ($R_{in}(t = t_1) = 0$). It is well known [10, 11] that $u_k$ grows exponentially:

$$u_k(t) = u_k(0) e^{v_s t / R_2(0)}, \tag{B.2}$$

where $v_s = \sigma/\eta$ is the characteristic speed and $R_2(0)$ the characteristic length scale of the system. We assume that $u_k$ grows exponentially all the way until breakup of the droplet. On the other hand we have shown that $R_{in}(t)$ decreases almost linearly in time. So formally, we have

$$R_{in}(t) = R_{in}(t = 0) - v_c t, \tag{B.3}$$

from which we have $t_1 = \frac{R_{in}(t=0)}{v_c}$. By inserting Eq.(B.2,B.3) into Eq.(B.1), we obtain

$$\frac{R_1(0)}{R_2(0)} \gtrsim 1 + c \ln(\frac{R_2(0)}{u_k(0)}), \tag{B.4}$$

where $c = v_c/v_s$ is an aspect ratio factor of order one that tends to 1/2 for aspect ratio one by Eq.(14). Thus the Rayleigh instability is dominant for sufficiently thin tori.

It can be checked that for aspect ratios satisfying Eq.(B.4) even the perimeter of the interior of the torus ($2\pi(R_1(0) - R_2(0))$) can accommodate the Rayleigh instability mode, i.e.,

$$\frac{2\pi(R_1(0) - R_2(0))}{R_2(0)} \gtrsim 2\pi \ln(\frac{R_2(0)}{u_k(0)}) > 2\pi. \tag{B.5}$$

### References

[1] P.G. de Gennes, F. Brochard-Wyart, and D. Quéré, *Capillarity and Wetting Phenomena:Drops, Bubbles, Pearls, Waves* (Springer, New York, 2003).

[2] R.V. Craster and O.K. Matar, Rev.Mod. Phys. **81**, 1131 (2009).

[3] T.M. Squires and S.R. Quake, Rev. Mod. Phys. **77**, 977 (2005).

[4] J. Eggers, Rev. Mod. Phys. **69**, 865 (1997).

[5] S. Chandrasekhar, *Hydrodynamic and Hydromagnetic Stability* (Clarendon Press, Oxford, 1961).

[6] M. Moseler and U. Landman, Science **289**, 1165 (2000).

[7] E.F. Goedde and M.C. Yuen, J. Fluid Mech. **40**, 495 (1970).

[8] H. Teng, C.M. Kinoshita, and S.M. Masutani, Int. J. Multiphase Flow **21**, 129 (1995).

[9] R.J. Donnelly and W. Glaberson, Proc. R. Soc. London, Ser. A **290**, 547 (1966).

[10] L. Rayleigh, Philos. Mag. **XXXIV**, 145 (1892).

[11] L. Rayleigh, Philos. Mag. **XXXIV**, 177 (1892).

[12] S.A. Safran, *Statistical Thermodynamics of Surfaces, Interfaces and Membranes* (Westview Press, Boulder, 2003).

[13] E. Pairam and A. Fernández-Nieves, Phys. Rev. Lett. **102**, 234501 (2009).

[14] S. Tomotika, Proc. R. Soc. London, Ser. A **150**, 322 (1935).

[15] J.D. McGraw *et al.*, Soft Matter **6**, 1258 (2010).

[16] M. Bowick, D.R. Nelson, and A. Travesset, Phys. Rev. E **69**, 041102 (2004).

[17] J. Vanderlinde, *Classical Electromagnetic Theory*, 2nd edition (Kluwer Academic Publisher, Dordrecht, 2004).

[18] L.D. Landau and E.M. Lifshitz, *Fluid Mechanics*, 2nd edition (Pergamon Press, Oxford, 1987).

[19] S.A. Khuri and A.M. Wazwaz, Appl. Math. Comput. **85**, 139 (1997).

[20] R.P. Feynman, R.B. Leighton, and M. Sands, *The Feynman Lectures on Physics, Volume 2* (Addison-Wesley Publishing Company, Massachusetts, 1964).